



Analytical and Numerical Simulation of Surface Pressure of an Oscillating Wedge at Hypersonic Mach Numbers and Application of Taguchi's Method

Shamitha¹, Asha Crasta¹, Khizar Ahmed Pathan², Sher Afghan Khan^{3,*}

¹ Department of Mathematics, M.I.T.E, Moodabidri & Affiliated To VTU, Belgavi, Karnataka, India

² Department of Mechanical Engineering, Trinity College of Engineering and Research, Pune, India

³ Department of Mechanical Engineering, Faculty of Engineering, IIUM, Gombak Campus, Kuala Lumpur, Malaysia

ARTICLE INFO

Article history:

Received 27 December 2022

Received in revised form 17 January 2023

Accepted 8 February 2023

Available online 2 March 2023

Keywords:

Hypersonic; Mach number; Wedge angle

ABSTRACT

This paper aims to estimate the surface pressure of a wedge at hypersonic Mach numbers at a considerable angle of incidence. The Ghosh similitude, corresponding strip theory, and piston theory are used to determine the pressure distribution analytically, and the results are compared to those of the CFD analysis. The theory is valid when the shock wave is attached to the leading edge of the nose of the wedge. Pressure on the windward surface was considered in the analysis. The pressure on the Lee surface is neglected. The condition for the validity of the theory is that the Mach number M_2 behind the shock wave is greater than 2.5. The parameters taken into account for the study are the wedge angle and Mach number. The range of wedge angle considered is from 5 to 25 degrees and the Mach number considered is from 5 to 15. The analytical and the CFD results are in good agreement. The findings indicate that the parameters like wedge angle and Mach number are influential parameters that influence the wedge surface static pressure. The surface static pressure rises with an increase in Mach number and wedge angle.

1. Introduction

The study of hypersonic flow continues to be an interesting area because of the latest developments of missiles, rockets, and launch vehicles for satellite launch at hypersonic Mach numbers. Most of the researchers have been trying to focus on aerodynamic heating problems in hypersonic flow. To accomplish this, we need to develop materials for the missile or launch vehicles and the propulsion systems at high speed. This has forced researchers to look for new materials study and injection of fuel into the combustion chamber at supersonic flow. It is mandatory on the part of the researchers to isolate the shockwaves by conducting a test to ensure that the flow is free from the shock waves during the fuel injections. At supersonic speed, our major concern is to have attached shock waves so that the wave drag is minimum. As aerodynamic heating is not a serious issue at supersonic speed rather we focus on the minimum drag of aerospace vehicles. While

* Corresponding author.

E-mail address: sakhan@iium.edu.my

<https://doi.org/10.37934/araset.30.1.1530>

developing the linearized theory the perturbation velocity component was very small as compared to the free stream velocity. The linearized theory was not valid when the Mach number is very close to unity as while developing the theory we neglected the second-order terms in comparison to the first-order terms.

The flow behavior of hypersonic flow differs from supersonic flow because it occurs at very high Mach numbers. In hypersonic flow, the perturbation velocity components are of the same order of magnitude as that of the free stream velocity. This is the major feature of the hypersonic flow that differentiate it from the supersonic flow. Aerodynamic heating is a serious issue. Once the Mach number is greater than 10 and above the surface temperature becomes very high.

The idea of an oscillating airfoil in pitch at a variety of Mach values was developed by Lighthill in 1953. By assuming that air is a perfect gas, Lighthill [1] was able to come up with an analytical answer for pitching symmetric airfoils. Hayes [2] explored unsteady flow with high Mach numbers over thin airfoils. Hui investigated and formed the precise solution for an oscillating wedge of 2D flow [3]. He then deduced the solutions for all supersonic Mach numbers and angles of attack while taking the associated shock wave into account for an oscillating flat plate. Liu & Hui [4] continued Hui's [3] theory for oscillating flat plate delta wings in pitch with attached shock waves.

The relationship between Lighthill [1] & Mile's, and Ghosh & Mistry's [5] piston theory for the order of two If the shock wave is attached, the angle between the plane and the shock generally relates to the windward surface [3-4]. Ghosh & Mistry [5] has discovered a similitude in hypersonic flow for delta wings with an associated leading edge shock at significant incidence [6]. Hui [3] studied, generated the exact solution in an oscillating wedge for a 2D flow, and obtained the solutions for all supersonic Mach numbers and angle of attack while taking into account the linked shock wave for an oscillating flat plate. Liu & Hui [4] continued Hui's [3] theory of oscillating flat plate delta wings in pitch with related shock waves in 1977.

Ghosh & Mistry [5] linked the ideas of Lighthill [1] with Mile's piston theory for orders of two and higher. Assuming the shock wave is attached, this angle is between the plane that roughly corresponds to the windward surface and the shock. Analytical and computational investigation of aerodynamic derivatives in an oscillating wedge is carried out by Khan *et.al.*, [7-10]. Pathan *et al.*, [11-12] have investigated the various shapes of boat tail helmets and human-power submarines to lower drag.

Mach numbers and wedge angles by computing various flow parameters for the planar wedge. The CFD study is used in conjunction with the wedge's angle, which spans from 5 to 25 degrees. Figure 1 shows the wedge geometry used for analysis and simulation. Where θ is the semi-vertex angle of the wedge, M is the freestream Mach number, and L is the slant length of the wedge.

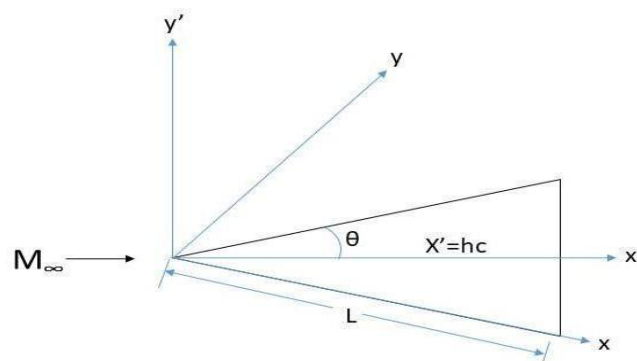


Fig. 1. Plane wedge geometry for changing the pivot's position from x_0 to x'_0

Consider the flat plate aerofoil of length L along with the mean wedge angle θ , which oscillates with low amplitude in pitch about the pivot position o_1 and is at a distance x_0 from its apex. At any instant, the angle of attack is α . Then the tiny piston velocity at point x is written in Eq. (1). The piston Mach number is given by Eq. (2).

$$U_p = U_\infty \sin \alpha + q(x - x_0) \quad (1)$$

$$M_p = M_\infty \sin \alpha + \frac{q(x-x_0)}{a_\infty} \quad (2)$$

Where;

M_p is the piston Mach number

M_∞ is the free stream Mach number

α is the angle of attack

q is the pitch rate

a_∞ is the free stream velocity

Lighthill [1] presented three components in the isentropic formulation for the pressure on a piston as in the power series with its velocity to relate the piston velocity and pressure on the piston surface. The piston velocity must be less than or equal to the free-stream sound velocity to meet the isentropic requirement. This is consistent with Lighthill's [1] idea of a modest hypersonic disturbance based on the piston theory.

The strip of wedge parallel to the center line can be assumed to be independent along the z-direction because the velocity component in the z-direction is minimal [5]. Surface pressure P can be directly coupled with the appropriate Mach number M_p' , and it integrates the strip theory with the considerable incidence similitude of Ghosh's results in the piston analogy [5]. The flow deflection and piston Mach number " M_p " are acceptable to large in the current scenario.

As a result, the Ghosh's piston hypothesis is employed rather than the Lighthill or Miles' strong shock piston theories. The inertia level at the piston M_p on the wing surface can directly be influenced by the surface pressure P. Eq. (3) provides the expression for pressure distribution.

$$\frac{P_2}{P_1} = 1 + A(M_p)^2 + AM_p \sqrt{B + (M_p)^2} \quad (3)$$

Where;

P_2 is pressure on the windward surface

P_1 is freestream pressure

Strips are regarded as being independent of one another at various span points. The wedge angle is the same as the wing angle. ' M_p ' and flow deflection are both permitted to be high in the current scenario. The piston theory taken into account in Eq. (3) can also be applied to supersonic flow, and the equation can now be written as Eq. (4).

$$\frac{P_2}{P_1} = 1 + A \left(\frac{M_p}{\cos \theta} \right)^2 + A \left(\frac{M_p}{\cos \theta} \right) \sqrt{B + \left(\frac{M_p}{\cos \theta} \right)^2} \quad (4)$$

Where;

\emptyset is the angle between the wing strip and the shock

$$A = \frac{\gamma(\gamma+1)}{4} \text{ and}$$

$$B = \left(\frac{4}{\gamma+1}\right)^2$$

2. Methodology

2.1 Taguchi Design

A Taguchi technique provides a way for experimentation that permits one to select a procedure that works most consistently in a working condition. Taguchi Designs understands that not all elements that cause deviation are controllable. Two factors Mach number and angle of incidence with five levels each are considered to create the Taguchi design. The Taguchi orthogonal array L25 shown in Table 1 is selected for the research work. A total of 25 trials are completed for CFD analysis and the response as dimensionless pressure values at the nose i.e. the static pressure at the nose of a 2D wedge divided by atmospheric pressure are included in Table 1.

Table 1
 Taguchi orthogonal array L25

Run	Factors		Response
	The angle of Incidence (Degrees)	Mach number	Pressure (P_2/P_1) at nose
1	5	5.5	1.590721
2	5	7	1.717036
3	5	9	1.876544
4	5	12	2.098904
5	5	15	2.330254
6	10	5.5	2.68322
7	10	7	3.136181
8	10	9	3.748542
9	10	12	4.714248
10	10	15	5.779966
11	15	5.5	4.469737
12	15	7	5.62678
13	15	9	7.143674
14	15	12	9.779799
15	15	15	12.96851
16	20	5.5	7.44499
17	20	7	9.658944
18	20	9	12.86536
19	20	12	18.63313
20	20	15	25.73121
21	25	5.5	10.40882
22	25	7	14.1656
23	25	9	19.97031
24	25	12	31.07335
25	25	15	45.0546

2.2 CFD Analysis

Utilizing ANSYS Workbench and Fluent, a computational fluid dynamics (CFD) analysis was carried out to validate the findings of the analytical work. The following Mach numbers are considered in the analysis: 5.5, 7, 9, 12, 15. The wedge angles that are considered are 5, 10, 15, 20, and 25 degrees. All possible parameter combinations for weak solutions are considered for CFD analysis. The fluid that represents air in the CFD analysis is an ideal gas.

2.2.1 Modeling

In the ANSYS design modeler, the wedge angle is varied to model all geometries. Figure 2 depicts the geometry for the 2D wedge and its enclosure. By taking into account the various wedge angles (θ), ranging from 5° to 25° , all geometries are modeled. For all models, length (L)=10 mm is taken into account. The enclosure of 3 times the length (L) front side, five times the length (L) rear side, and five times the length (L) at the top and bottom sides are created for CFD analysis. The inlet and outlet names are given to the front and rear edges, as shown in Figure 2.

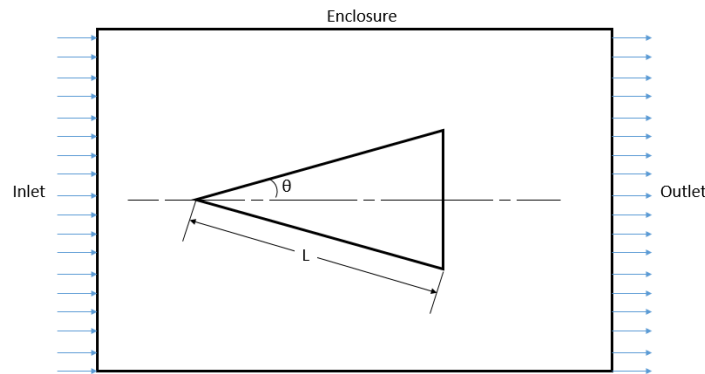


Fig. 2. 2D geometry of wedge and enclosure

2.2.2 Meshing

Finding the ideal mesh element size requires performing the grid independence test before meshing. The grid independence test has been performed for Mach number 7 and 20° wedges with mesh sizes ranging from 1 mm to 10 mm. The number of elements and nodes for mesh sizes ranging from 4mm to 1mm is shown in Table 2.

Table 2

Grid independence test: number of mesh elements with various element sizes

Mesh Element Size (mm)	No. of Mesh Nodes	No. of Mesh Elements
10	11412	11114
9	13542	13223
8	16828	16482
7	21281	20902
6	28361	27932
5	39924	39429
4	60600	60013
3	107696	106939
2	240144	239070
1	972997	970927

The grid independence test results are shown in Figure 3. It is obvious from the findings that for a mesh element size of 5 mm, the result is stable, and the mesh element size of 5 mm can be taken into consideration for the CFD analysis. For subsequent CFD studies, a mesh element size of 2 mm is used for higher precision.

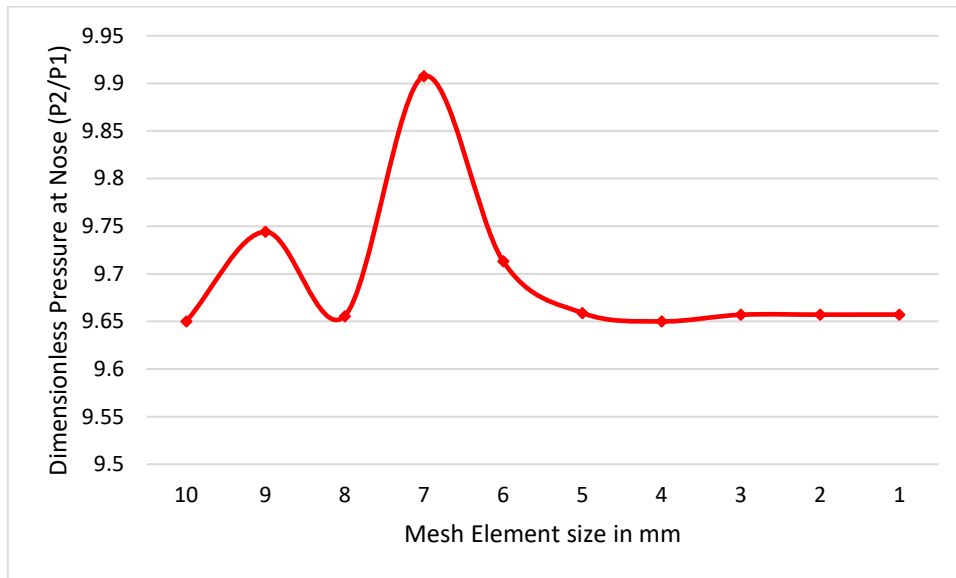


Fig. 3. Grid independence test

The hexahedral mesh elements are used in the meshing. Figure 4(a) shows the complete meshed model, and Figure 4(b) shows the enlarged view of the wedge geometry.

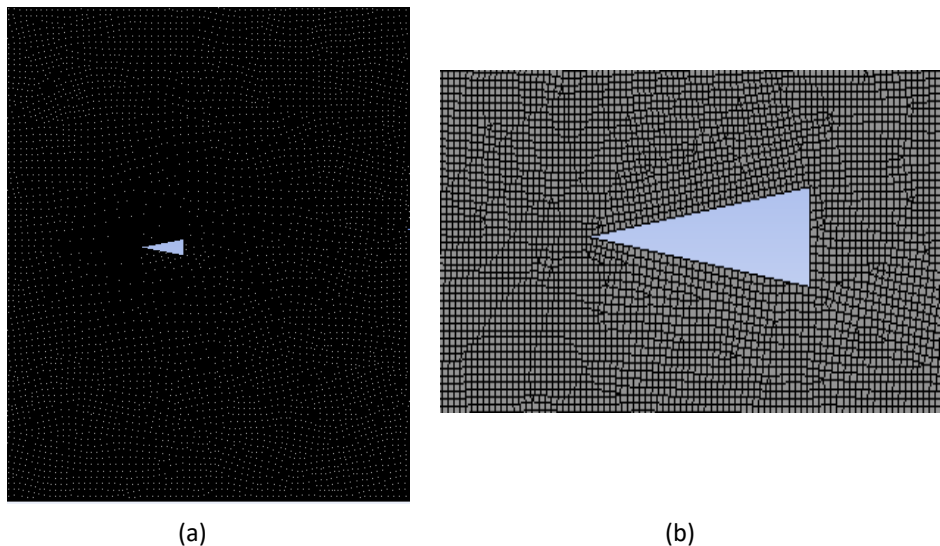


Fig. 4. 2D meshed geometry for $\theta=15^\circ$ and mesh element size 4mm (a) Complete geometry (b) Enlarged view of the wedge

2.2.3 CFD analysis

The CFD analysis is carried out for all possible parameter combinations. The k-epsilon turbulent model is employed for analysis which is more suitable and reliable turbulent model in variety of applications [13-31]. Inlet is a velocity inlet, and outflow is a pressure outlet for the boundary conditions. After setting the boundary conditions, the solution is initialized, and at least 10,000

iterations are run. In many instances within 1000 iterations, the solution appeared to have converged.

3. Results and Discussion

Analytical findings and CFD results are found to be in very good agreement. The analytical results and CFD analysis's highest degree of divergence is 10%. The results are explained in the following sections.

3.1 Main Effects Plots for Dimensionless Static Pressure

The major effect map for dimensionless static pressure at the wedge's nose is shown in Figure 5. The mean values of pressure for all cases are considered and plotted in Figure. 5. According to the results, as the Mach number increases, so does the static pressure at the nose due to the increase in the inertia values and hence the strength of the oblique shock wave. A progressive increase in the pressure ratio is observed. It is well known that the pressure ratio after and before the shock wave is a measure indicating the strength of the shock wave located at the nose. Across the shock waves, the stagnation pressure and temperature before and after the shock waves are identical. From the main effects plot, it is seen that the pressure ratio at Mach 5.5, 7, 9, 12, and 15 are 5.8, 7.4, 9.5, 13.6, and 18.3.

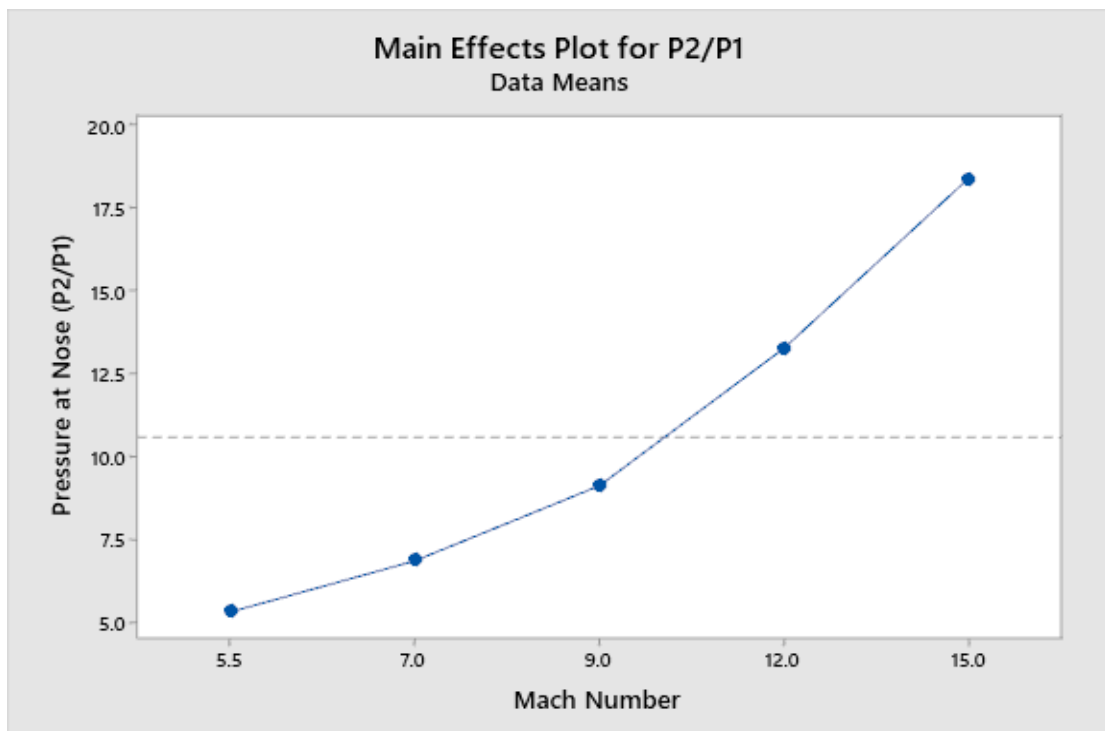


Fig. 5. Main effect of Mach number on dimensionless static pressure (P_2/P_1) at the nose of wedge

3.2 Main Effects Plots for Dimensionless Static Pressure

Figure 6 shows the main effect plot for dimensionless static pressure at the nose of the wedge. Based on the obtained results, the static pressure at the nose increases with an increase in the wedge angle. The major effect map for dimensionless static pressure at the wedge's nose is depicted in

Figure 6. According to the data, as the wedge semi-vertex angle increases, so does the static pressure at the nose. With the progressive increase in the semi-vertex angle the surface area of the wedge increases. This increase in the surface area of the wedge will result in totally different pressure and hence the larger value of the pressure ratio. From Figure. 6 it is seen that when semi-vertex angle $\theta = 5, 10, 15, 20,$ and 25 degrees the corresponding surface pressure ratios are $2.6, 4.8, 8.4, 15.2,$ and 23.9 . These results reiterate that the surface pressure ratio also increases with the increase in the semi-vertex angle of the wedge. The increase in the pressure ratio is almost linear.

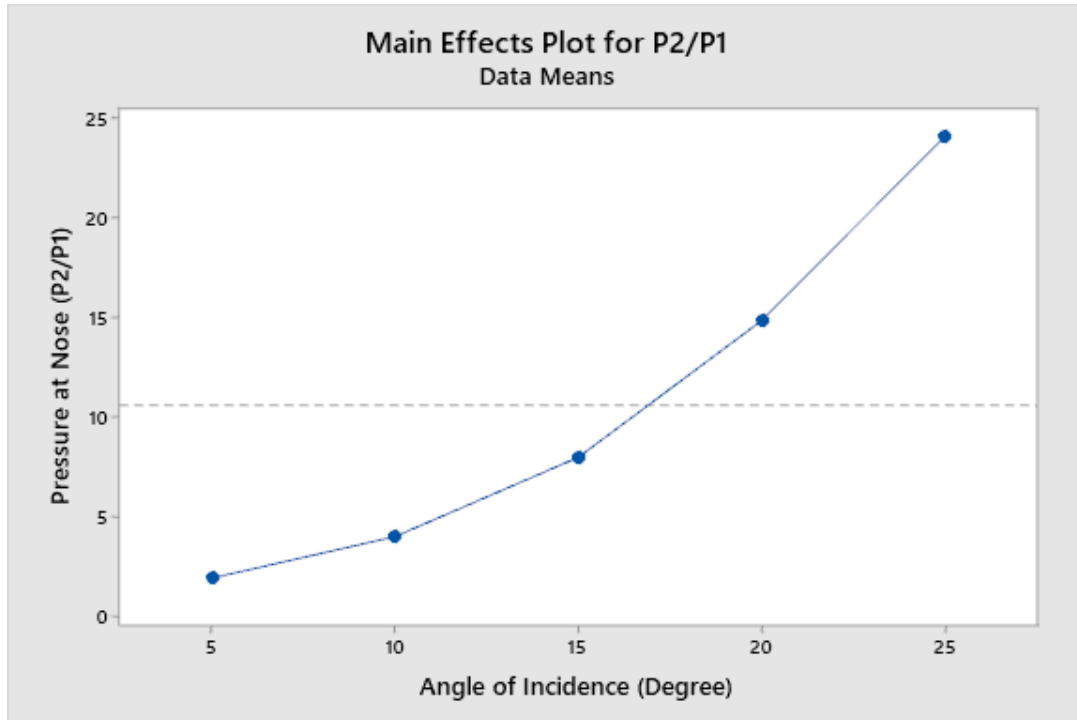


Fig. 6. Main effect of angle of incidence on dimensionless static pressure (P_2/P_1) at the nose of wedge

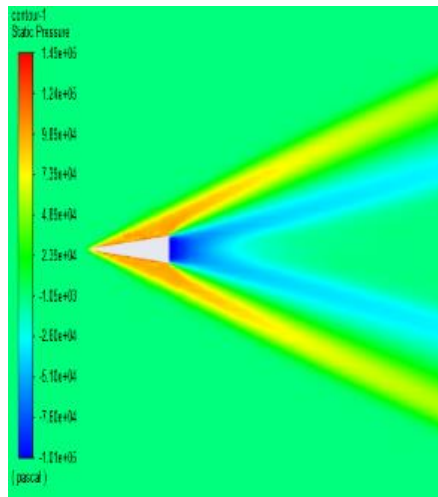
3.3 The Pressure Contour for Static Pressure

In Figure 7, which displays the static pressure contours for various Mach numbers and angles of incidence, it can be seen that as Mach increases, the Mach cone angle decreases. The base region grows as the wedge angle increases. From the results, it is seen that as the Mach number increases with the same wedge angle, the Mach angle reduces. If the shock is extremely weak, the Mach angle (μ) is the same as the. Theoretically, the Mach angle (μ) is given by Eq. (5) [28].

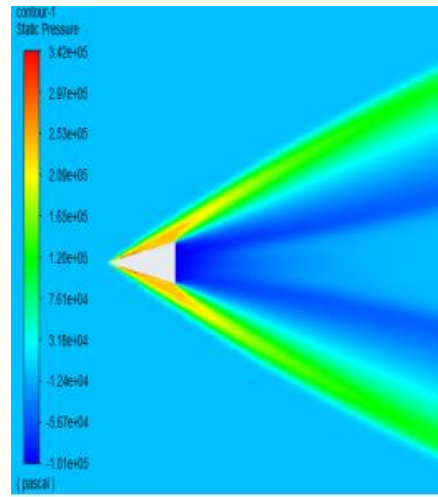
$$\mu = \sin^{-1}\left(\frac{1}{M}\right) \quad (5)$$

It is also seen that as the angle of incidence increases, the Mach angle increases. The relation between the angle of incidence (θ), shock angle (β), and Mach number (M) is given by Eq. (6) [28].

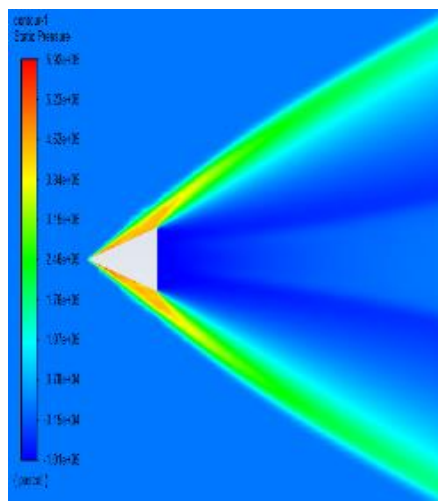
$$\tan\theta = 2\cot\beta \left(\frac{M_1^2 \sin^2\beta - 1}{M_1^2 (\gamma + \cos 2\beta) + 2} \right) \quad (6)$$



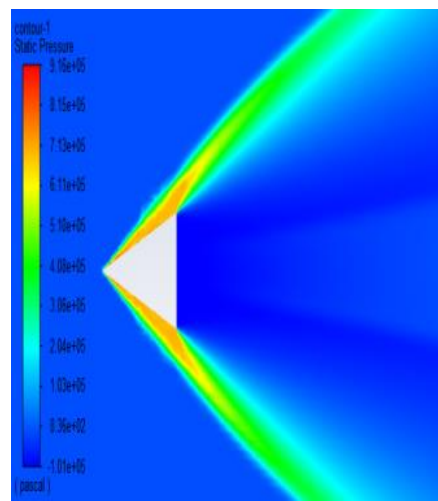
(a) $M=5.5, \theta=5^\circ$



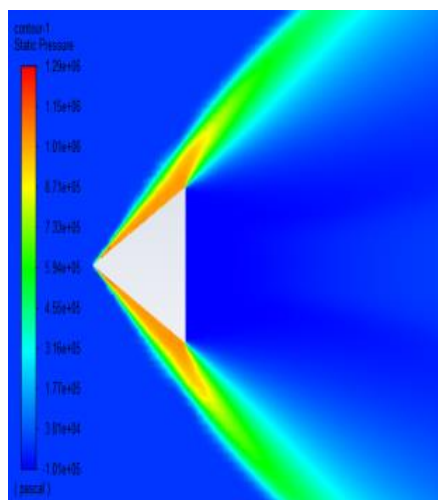
(b) $M=5.5, \theta=10^\circ$



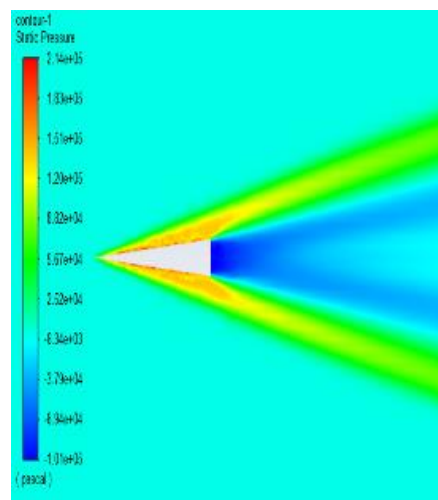
(c) $M=5.5, \theta=15^\circ$



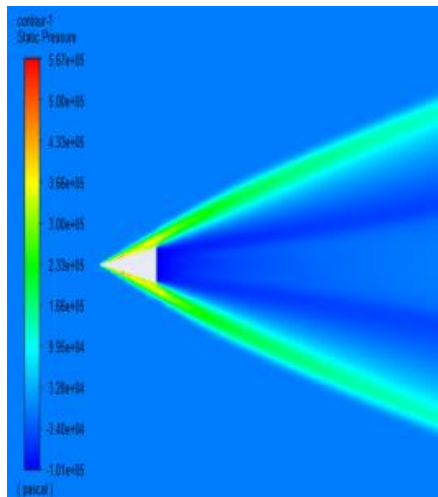
(d) $M=5.5, \theta=20^\circ$



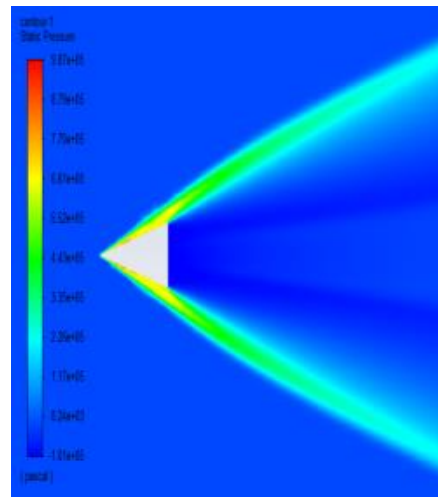
(e) $M=5.5, \theta=25^\circ$



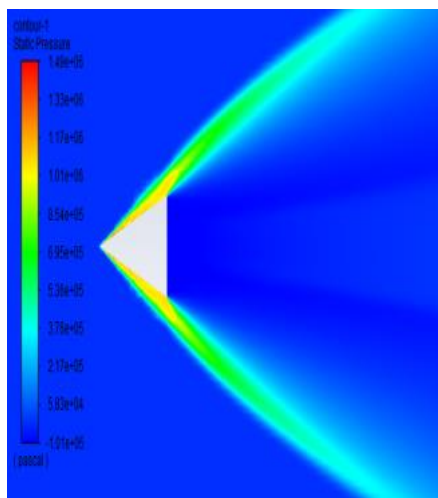
(g) $M=7, \theta=5^\circ$



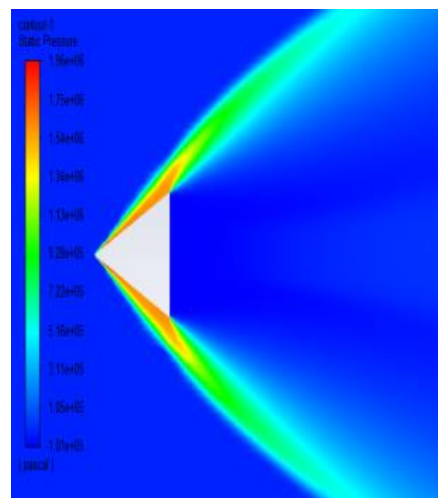
(h) $M=7, \theta=10^\circ$



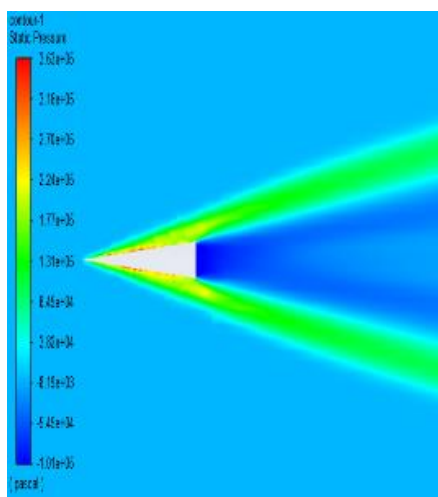
(i) $M=7, \theta=15^\circ$



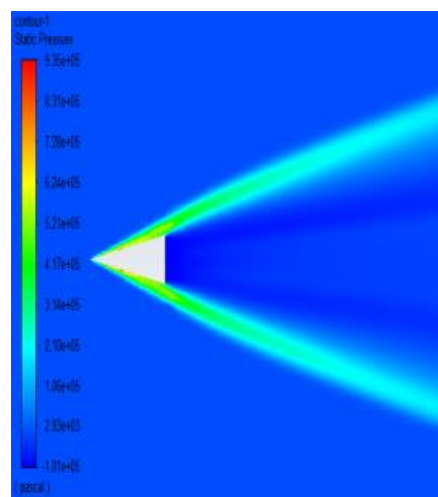
(j) $M=7, \theta=20^\circ$



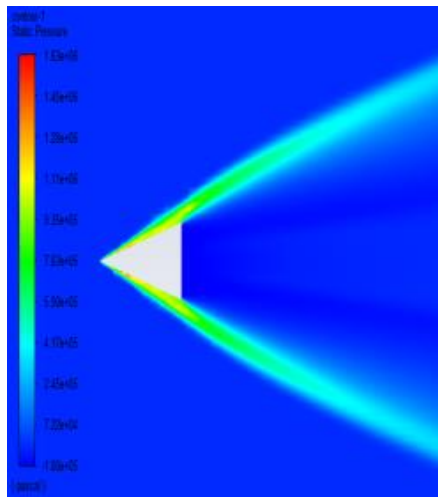
(k) $M=7, \theta=25^\circ$



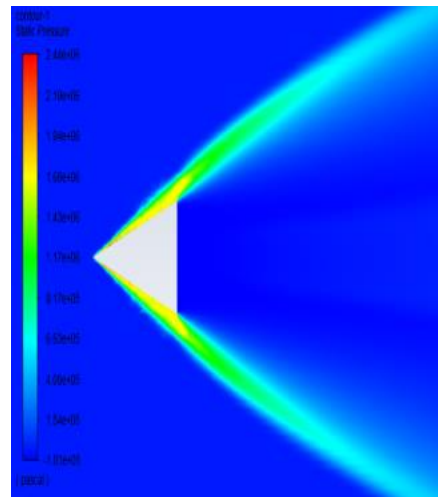
(l) $M=9, \theta=5^\circ$



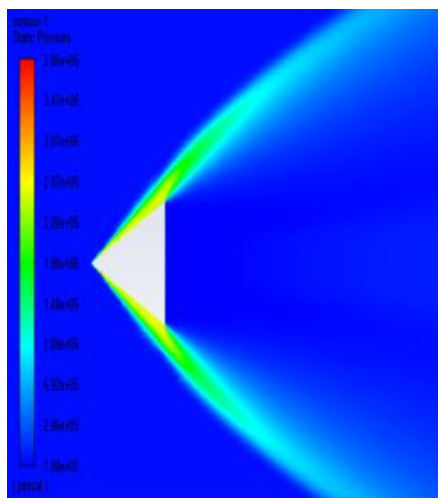
(m) $M=9, \theta=10^\circ$



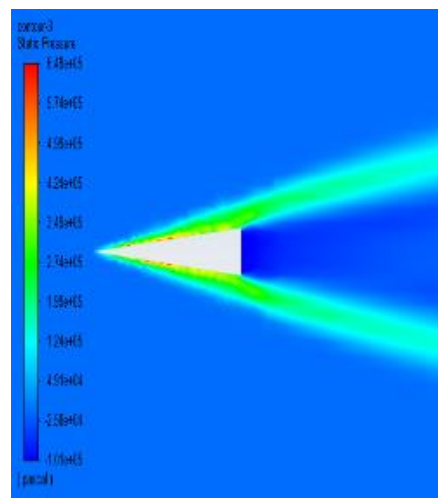
(n) $M=9, \theta=15^\circ$



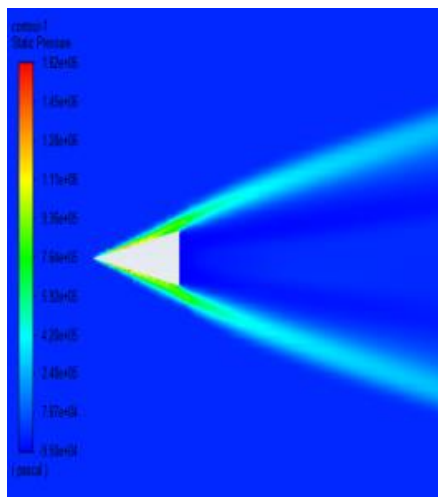
(o) $M=9, \theta=20^\circ$



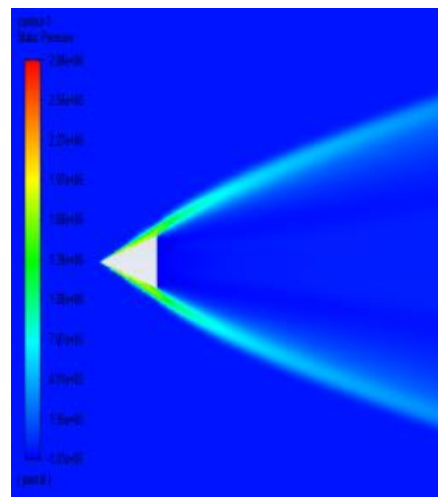
(p) $M=9, \theta=25^\circ$



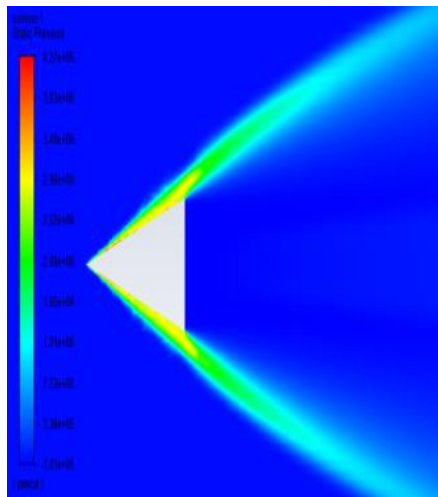
(q) $M=12, \theta=5^\circ$



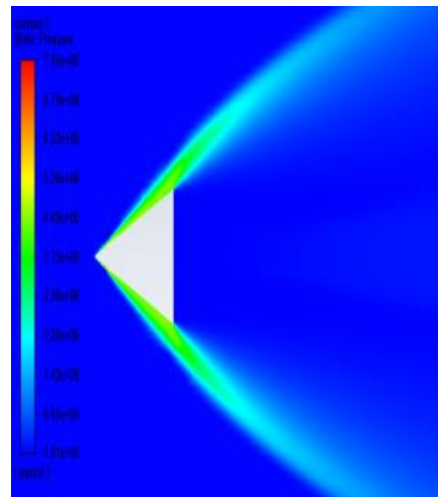
(r) $M=12, \theta=10^\circ$



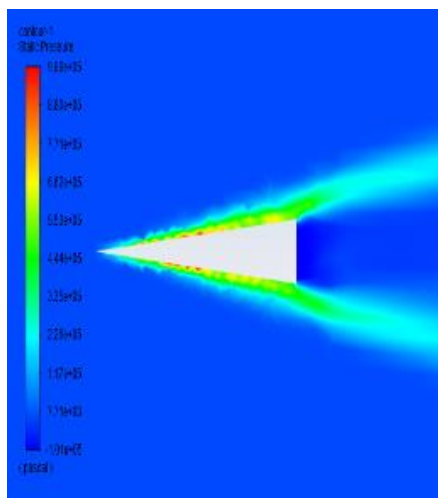
(s) $M=12, \theta=15^\circ$



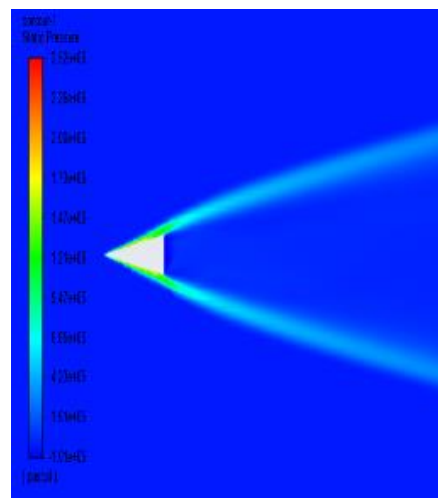
(t) $M=12, \theta=20^\circ$



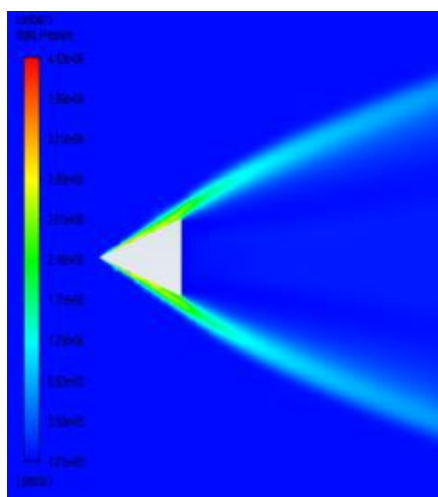
(u) $M=12, \theta=25^\circ$



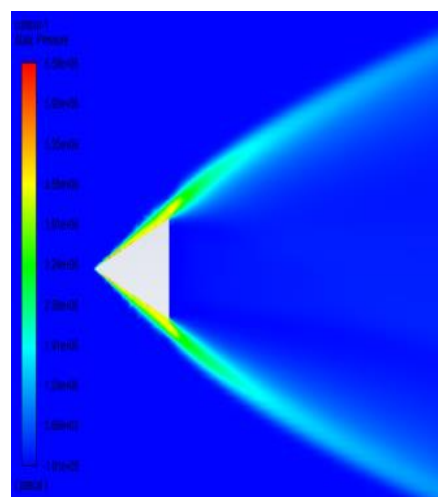
(v) $M=15, \theta=5^\circ$



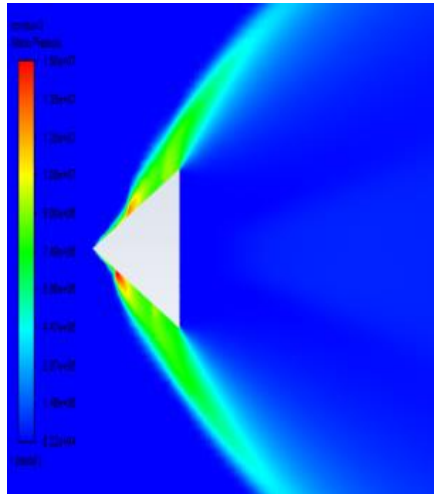
(w) $M=15, \theta=10^\circ$



(x) $M=15, \theta=15^\circ$



(y) $M=15, \theta=20^\circ$



(z) M=15, $\theta=25^\circ$

Fig. 7. Contours of static pressure for various Mach numbers and angle of incidences

3.4 The Effect of Mach Number on Pressure at the Nose

Figure 8 shows the variations of dimensionless static pressure at the nose of the wedge versus Mach and numbers for various angles of incidence. The obtained results clearly show that the CFD and analytical results have an excellent agreement. The absolute static pressure is divided by atmospheric pressure to non-dimensionalized pressure as the Mach number increases, the dimensionless pressure increases. For the lower wedge angle, i.e., $\theta = 5^\circ$ and 25° , the change in pressure at the nose is marginal with an increase of Mach number from 5.5 to 15. As the wedge angle increases, the effectiveness of the Mach number increases, and the change of pressure at the nose considerably increases.

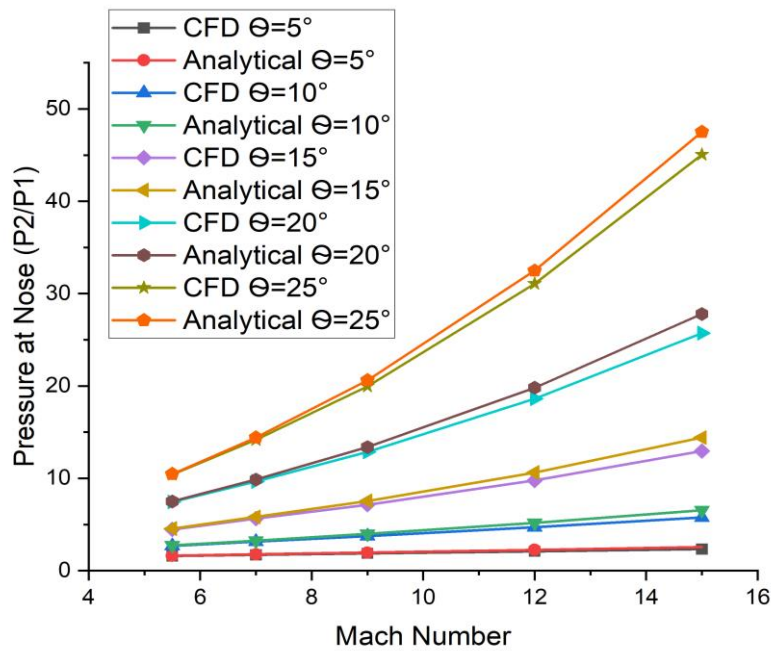


Fig. 8. Variations of dimensionless static pressure at the nose of the wedge versus Mach numbers

3.5 The Effect of Angle of Incidence on Pressure at the Nose

Figure 9 shows the variations of dimensionless static pressure at the nose of the Wedge Vs. wedge angle for various Mach numbers for the hypersonic Mach number, with increasing wedge angle, there is a significant increase in the variation of dimensionless static pressure at the wedge's nose.

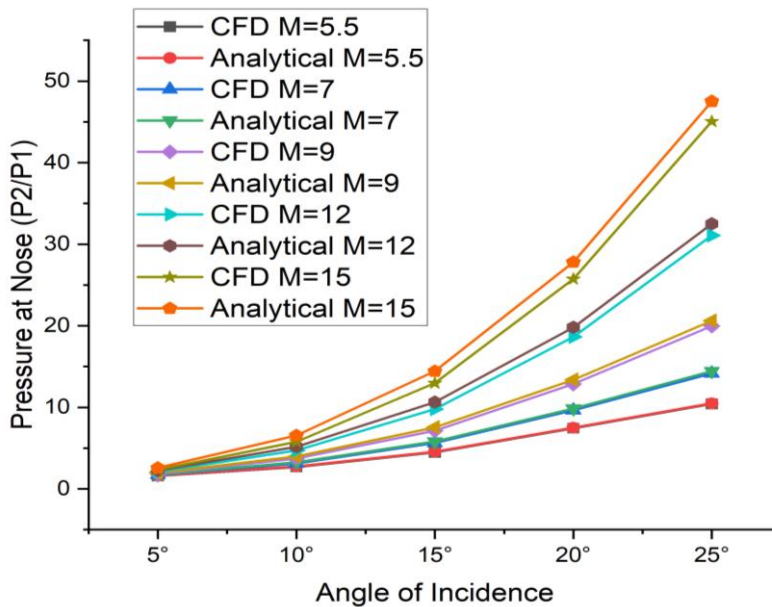


Fig. 9. Variation of dimensionless pressure versus angle of incidence

3.6 The Contour Plot of Dimensionless Pressure at the Nose

The contour plot for the pressure at the nose is shown in Figure 10. Based on the contour plot it can be observed that the pressure on the nose of the 2D wedge increases with an increase in Mach number as well as the angle of incidence. The pressure on the nose has a maximum value of larger than 44 times the atmospheric pressure at Mach number close to 15 and an angle of incidence of close to 25 degrees.

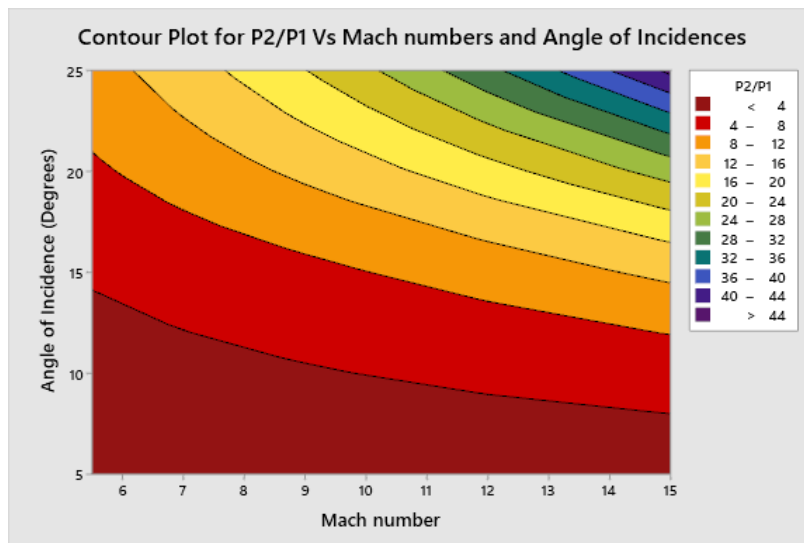


Fig. 10. Contour plot of dimensionless pressure at nose versus Mach number and angle of incidence

4. Conclusions

The Ghosh piston theory is used to calculate the pressure distribution analytically, and the outcomes are then compared to those of the CFD analysis. The outcomes and the CFD and analytical results are in excellent agreement have been discovered that the variation of dimensionless pressure is influenced by both the Mach number and the wedge angle. It is also noted that for lower wedge angles and lower Mach numbers, the dimensionless static pressure at the wedge's nose only slightly alters. Given the high cost of wind tunnel tests, these findings are helpful when designing aerospace vehicles. As a result, these discoveries can be used to enhance aerospace vehicle design. The results of the current study are reliable and have impressive computational simplicity.

Acknowledgment

We gratefully thank the Management and Mangalore Institute of Technology and Engineering for their continuous support of our research work.

References

- [1] Lighthill, Mo J. "Oscillating airfoils at high Mach number." *Journal of the Aeronautical Sciences* 20, no. 6 (1953): 402-406. <https://doi.org/10.2514/8.2657>
- [2] Hayes, Wallace D. "On hypersonic similitude." *Quarterly of Applied Mathematics* 5, no. 1 (1947): 105-106. <https://doi.org/10.1090/qam/20904>
- [3] Hui, W. H. "Supersonic and hypersonic flow with attached shock waves over delta wings." *Proceedings of the Royal Society of London. A. Mathematical and Physical Sciences* 325, no. 1561 (1971): 251-268. <https://doi.org/10.1098/rspa.1971.0168>
- [4] Liu, D. D., and W. H. Hui. "Oscillating delta wings with attached shock waves." *AIAA Journal* 15, no. 6 (1977): 804-812. <https://doi.org/10.2514/3.7371>
- [5] Ghosh, Kunal, and Binoy Krishna Mistry. "Large incidence hypersonic similitude and oscillating nonplanar wedges." *AIAA Journal* 18, no. 8 (1980): 1004-1006. <https://doi.org/10.2514/3.7702>
- [6] Ghosh, Kunal. "Hypersonic large-deflection similitude for oscillating delta wings." *the Aeronautical journal* 88, no. 878 (1984): 357-361.
- [7] Khan, Sher Afghan, Abdul Aabid, and C. Ahamed Saleel. "CFD simulation with analytical and theoretical validation of different flow parameters for the wedge at supersonic Mach number." *International Journal of Mechanical and Mechatronics Engineering* 1 (2019).
- [8] Crasta, Asha, and S. A. Khan. "Hypersonic similitude for planar wedges." *International Journal of Advanced Research in Engineering and Technology* 5, no. 2 (2014): 16-31.
- [9] Crasta, Asha, and S. A. Khan. "High Incidence Supersonic similitude for Planar wedge." *International Journal of Engineering research and Applications* 2, no. 5 (2012): 468-471.
- [10] Shaikh, Javed S., Krishna Kumar, Khizar A. Pathan, and Sher A. Khan. "Analytical and computational analysis of pressure at the nose of a 2D wedge in high speed flow." *Advances in aircraft and spacecraft science* 9, no. 2 (2022): 119-130. <https://doi.org/10.12989/aas.2022.9.2.119>
- [11] Pathan, Khizar A., Sher A. Khan, N. A. Shaikh, Arsalan A. Pathan, and Shahnawaz A. Khan. "An investigation of boat-tail helmet to reduce drag." *Adv. Aircr. Spacecr. Sci* 8 (2021): 239-250.
- [12] Khan, Sher Afghan, M. A. Fatepurwala, and K. N. Pathan. "CFD analysis of human powered submarine to minimize drag." *Ratio (L/D)* 4 (2018): 5. <https://doi.org/10.24247/ijimperdjun2018111>
- [13] Pathan, Khizar Ahmed, Prakash S. Dabeer, and Sher Afghan Khan. "Influence of expansion level on base pressure and reattachment length." *CFD Letters* 11, no. 5 (2019): 22-36.
- [14] Pathan, Khizar Ahmed, Syed Ashfaq, Prakash S. Dabeer, and Sher Afgan Khan. "Analysis of parameters affecting thrust and base pressure in suddenly expanded flow from nozzle." (2019).
- [15] Pathan, Khizar, Prakash Dabeer, and Khan Sher. "An investigation of effect of control jets location and blowing pressure ratio to control base pressure in suddenly expanded flows." *Journal of Thermal Engineering* 6, no. 2 (2019): 15-23. <https://doi.org/10.18186/thermal.726106>
- [16] Pathan, Khizar Ahmed, Prakash S. Dabeer, and Sher Afghan Khan. "Effect of nozzle pressure ratio and control jets location to control base pressure in suddenly expanded flows." *Journal of Applied Fluid Mechanics* 12, no. 4 (2019): 1127-1135. <https://doi.org/10.29252/jafm.12.04.29495>

- [17] Pathan, Khizar Ahmed, Prakash S. Dabeer, and Sher Afghan Khan. "An investigation to control base pressure in suddenly expanded flows." *International Review of Aerospace Engineering (I. RE. AS. E)* 11, no. 4 (2018): 162-169. <https://doi.org/10.15866/irease.v11i4.14675>
- [18] Pathan, Khizar Ahmed, Prakash S. Dabeer, and Sher Afghan Khan. "Optimization of area ratio and thrust in suddenly expanded flow at supersonic Mach numbers." *Case studies in thermal engineering* 12 (2018): 696-700. <https://doi.org/10.1016/j.csite.2018.09.006>
- [19] Pathan, Khizar Ahmed, Sher Afghan Khan, and P. S. Dabeer. "CFD analysis of effect of flow and geometry parameters on thrust force created by flow from nozzle." In *2017 2nd International Conference for Convergence in Technology (I2CT)*, pp. 1121-1125. IEEE, 2017. <https://doi.org/10.1109/I2CT.2017.8226302>
- [20] Pathan, Khizar Ahmed, Sher Afghan Khan, and P. S. Dabeer. "CFD analysis of effect of area ratio on suddenly expanded flows." In *2017 2nd International Conference for Convergence in Technology (I2CT)*, pp. 1192-1198. IEEE, 2017. <https://doi.org/10.1109/I2CT.2017.8226315>
- [21] Pathan, Khizar Ahmed, Sher Afghan Khan, and P. S. Dabeer. "CFD analysis of effect of Mach number, area ratio and nozzle pressure ratio on velocity for suddenly expanded flows." In *2017 2nd International Conference for Convergence in Technology (I2CT)*, pp. 1104-1110. IEEE, 2017. <https://doi.org/10.1109/I2CT.2017.8226299>
- [22] Pathan, Khizar A., Prakash S. Dabeer, and Sher A. Khan. "Enlarge duct length optimization for suddenly expanded flows." *Advances in Aircraft and Spacecraft Science* 7, no. 3 (2020): 203-214.
- [23] Shaikh, Sohel Khalil, Khizar Ahmed Pathan, Zakir Ilahi Chaudhary, B. G. Maripalle, and Sher Afghan Khan. "An Investigation of Three-Way Catalytic Converter for Various Inlet Cone Angles Using CFD." *CFD Letters* 12, no. 9 (2020): 76-90. <https://doi.org/10.37934/cfdl.12.9.7690>
- [24] Shaikh, Sohel Khalil, Khizar Ahmed Pathan, Zakir Ilahi Chaudhary, and Sher Afghan Khan. "CFD analysis of an automobile catalytic converter to obtain flow uniformity and to minimize pressure drop across the monolith." *CFD Letters* 12, no. 9 (2020): 116-128. <https://doi.org/10.37934/cfdl.12.9.116128>
- [25] Pathan, Khizar Ahmed, Prakash S. Dabeer, and Sher Afghan Khan. "Investigation of base pressure variations in internal and external suddenly expanded flows using CFD analysis." *CFD Letters* 11, no. 4 (2019): 32-40.
- [26] Shaikh, Javed S., Krishna Kumar, Khizar A. Pathan, and Sher A. Khan. "Computational Analysis of Surface Pressure Distribution over a 2D Wedge in the Supersonic and Hypersonic Flow Regimes."
- [27] Shamitha, Asha Crasta, Khizar Ahmed Pathan, and Sher Afghan Khan. "Numerical Simulation of Surface Pressure of a Wedge at Supersonic Mach Numbers and Application of Design of Experiments."
- [28] Rathakrishnan, Ethirajan. *Gas Dynamic*. Seventh ed. Delhi, Delhi: PHI Learning, 2020.
- [29] Kanaani, Osamah Othman, Sami Abdelrahman Musa Yagoub, Shabir Habib, Akmal Aulia, and Bonavian Hasiholan. "Prediction of gas coning in hydrocarbon reservoir using tNavigator." *Progress in Energy and Environment* 18 (2021): 1-22. <https://doi.org/10.37934/progee.18.1.122>
- [30] Nazer, Mohamed, Muhammad Fadzrul Hafidz Rostam, Se Yong Eh Noum, Mohammad Taghi Hajibeigy, and Kamyar Shameli. "Performance Analysis of Photovoltaic Passive Heat Storage System with Microencapsulated Paraffin Wax for Thermoelectric Generation." *Journal of Research in Nanoscience and Nanotechnology* 1, no. 1 (2021): 75-90. <https://doi.org/10.37934/jrnn.1.1.7590>
- [31] Elfaghi, Abdulhafid MA, Alhadi A. Abosbaia, Munir FA Alkibir, and Abdoulhdi AB Omran. "CFD Simulation of Forced Convection Heat Transfer Enhancement in Pipe Using Al₂O₃/Water Nanofluid." *Journal of Advanced Research in Numerical Heat Transfer* 8, no. 1 (2022): 44-49. <https://doi.org/10.37934/cfdl.14.9.118124>